Determination of absorption coefficients for concentrated samples by fluorescence detection

S. Eisebitt, T. Böske, J.-E. Rubensson, and W. Eberhardt
Institut für Festkörperforschung, Forschungszentrum Jülich, Postfach 1913, D-5170 Jülich, Germany
(Received 4 December 1992)

A method to determine the absorption coefficient near the onset of core-electron transitions for concentrated samples using fluorescence-yield (FY) detection is presented. Measuring the FY signal for different experimental geometries, we are able to calculate the true absorption coefficient. Thus we are able to correct fully for saturation effects present in FY spectra of concentrated samples. The technique is demonstrated for Co and a buried layer of $CoSi_2$.

I. INTRODUCTION

The x-ray-absorption near-edge structure (XANES) in the soft-x-ray region is in most cases monitored by electron yield (EY). Because of the limited escape depth of the electrons, the EY spectra do not reflect bulk properties but are largely dominated by surface effects. Though the escape depth can be varied in EY measurements by choosing an energy window in the partial-yield mode, tedious sample preparations are necessary to minimize effects produced by adsorbates. For most materials even the clean surface contribution cannot be neglected. This problem has been recognized, e.g., in the study of high-T_c superconductors, where unambigious XANES results cannot be achieved using EY methods.[1] EY techniques are, for the same reason, not well suited to study buried structures. Fluorescence-yield (FY) detection has recently been introduced as a technique for the study of real bulk properties. As Jaklevic *et al.*[2] pointed out, this technique of recording x-ray absorption is especially useful in the investigation of dilute samples and thin layers. In these cases the FY signal is directly proportional to the absorption coefficient in question. Additionally, the signal-to-background ratio is higher in FY than in EY measurements of dilute samples and FY detection can easily be used in the presence of magnetic fields, e.g., in measurements of the magnetic circular dichroism. For concentrated bulk samples, however, the measured FY is not proportional to the absorption coefficient. The experimental FY spectra exhibit distortions due to so-called "self-absorption effects".[2–4] These distortions vary with the geometry of the experiment. They are caused by the absorption of both the exciting photons on their way *into* the sample and the absorption of the generated fluorescence radiation on its way *out* of the sample.

The effect is illustrated in Fig. 1. In a grazing-incidence geometry as shown in Fig. 1(b), all incoming photons are absorbed close to the sample surface compared to the photon penetration length. If the electron transition investigated dominates the absorption, nearly all generated fluorescence photons will be able to escape out of the sample into the detector in a normal takeoff setup, as their way through the sample is short compared to the penetration length. Consequently, the signal is nearly independent of the absorption coefficient, which we intend to measure in a XANES experiment. We note that all techniques that take advantage of a large escape depth to

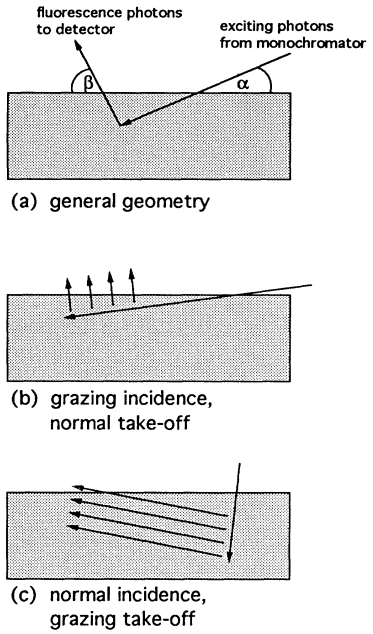

FIG. 1. In this figure we illustrate the influence of the experimental geometry upon the saturation effects observed in the FY. (a) shows the general geometry: Radiation from the monochromator enters the sample under the glancing angle α and may give rise to fluorescence radiation from the sample. The fluorescence radiation is detected under the angle β. In our setup $\alpha + \beta = 90°$. (b) shows the grazing-incidence normal-takeoff limit. If the electron transition investigated dominates the absorption, nearly all generated fluorescence photons contribute to the signal. Now the signal is nearly independent of the absorption coefficient of the sample and thus saturated. In the normal-incidence grazing-takeoff limit presented in (c), the signal becomes more and more proportional to the absorption coefficient *because* of the self-absorption experienced by the outgoing fluorescence photons, as fluorescence radiation generated deep in the sample cannot reach the detector.

monitor bulk properties share this problem. As the spectrum appears to be saturated, this effect is sometimes adressed as "saturation effect" in FY spectra. This is simulated in Fig. 2 for the Co $L_{2,3}$ edges.

In the normal-incidence grazing-takeoff limit as shown in Fig. 1(c), however, the signal becomes more and more proportional to the absorption coefficient. The absorption of the generated fluorescence radiation on the way out of the sample attenuates the fluorescence radiation. If the absorption coefficient of the sample is high, most fluorescence radiation will be produced close to the surface; consequently the detected signal is high. If the absorption coefficient is low, a larger amount of the fluorescence is produced in deeper regions of the sample, thus contributing less to the detected signal.

So it is qualitatively clear that the saturation effects in the FY signal become weaker in a normal-incidence grazing-takeoff geometry. However, we want to add that the term "self-absorption effect" used to explain the distortions in the grazing-incidence FY spectra is misleading, as the *lack* of self-absorption produces saturation.

For the x-ray-absorption fine-structure (EXAFS) energy range, the saturation effects can be corrected for using the information of the smooth background of the long data set.[5] This is impossible on the short energy interval of interest in XANES. A normal-incidence grazing-takeoff geometry has been used to record XANES spectra as the saturation effects can be reduced in such a geometry.[4] However, in practice it is difficult to know whether the saturation effects are fully eliminated at the chosen geometry.

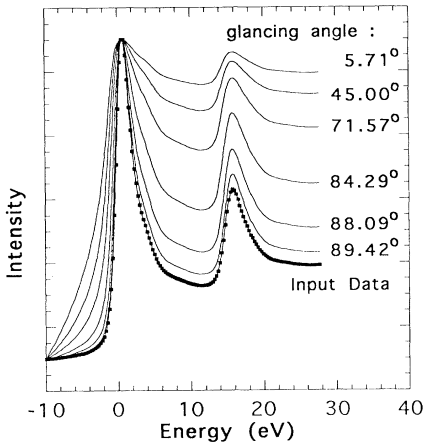

FIG. 2. Simulation of Eq. (1), demonstrating the saturation effects observed in x-ray-absorption spectra of concentrated samples detected by FY. The energy is measured relative to Co $2p_{\frac{3}{2}}$ electron binding energy. The calculations were carried out for Co using EY data as input (squares). It was assumed that $\mu_{\text{other}} = \text{const} = \mu_{\text{tot}}(E_f)$, where the constant is 14% of the rise of the absorption coefficient over the $L_{2,3}$ edges (Refs. 7 and 8). The intensities were calculated for geometry factors g of 0.1 (5.71°), 1 (45.00°), 3 (71.57°), 10 (84.29°), 30 (88.09°), and 100 (89.42°) and scaled to the L_3 peak for better comparison. See Sec. IV for a detailed discussion.

We report a different approach to determine the absorption of concentrated bulk samples by FY detection. As the absorption of the photons and the angular dependence can be described analytically, it is possible to determine the specific absorption coefficient of interest by analyzing FY spectra recorded at different angles.

II. THEORY

Consider a flat sample with thickness d oriented as shown in Fig. 1. Photons of energy E enter the sample with incident glancing angle α and can produce a core hole in a level X if their energy is sufficiently high. With the probability ω_X the hole decays by the emission of a photon with energy E_f. If the photon leaves the sample, it can be detected at takeoff angle β by the detector with efficiency η. Let μ_X be the absorption coefficient associated with the production of a core hole in the investigated level X; $\mu_{\text{tot}} = \mu_X + \mu_{\text{other}}$ is the total absorption coefficient of the sample, while μ_{other} describes absorption due to shallower core levels, valence levels, and other atomic species. The measured intensity is given by[2]

$$I^X(E) = \eta \frac{A}{r^2} \omega_X I_0(E) \frac{\mu_X(E)}{\mu_{\text{tot}}(E) + \mu_{\text{tot}}(E_f)\frac{\sin\alpha}{\sin\beta}} \times \left[1 - e^{-\left(\frac{\mu_{\text{tot}}(E)}{\sin\alpha} + \frac{\mu_{\text{tot}}(E_f)}{\sin\beta}\right)d}\right] \quad . \tag{1}$$

$I_0(E)$ denotes the intensity of the incoming light, A is the active detector area, and r is the distance to the sample. The formula reflects the facts that the incident radiation is absorbed according to $\mu_{\text{tot}}(E)$ and that the absorption of the produced fluorescence radiation with the unique energy E_f is characterized by $\mu_{\text{tot}}(E_f)$. It is derived by integrating the law of absorption with the corresponding absorption coefficients over the paths of the photons through the sample. The variation of β due to the solid angle A/r^2 covered by the detector is assumed to be small.

Thick samples are characterized by

$$e^{-\left(\frac{\mu_{\text{tot}}(E)}{\sin\alpha} + \frac{\mu_{\text{tot}}(E_f)}{\sin\beta}\right)d} \ll 1 \quad ; \tag{2}$$

i.e., the sample is thick with respect to the photon penetration depth. In this limit the exponential term can be neglected and the measured intensity is given by

$$I^X(E) = \eta \frac{A}{r^2} \omega_X I_0(E) \frac{\mu_X(E)}{\mu_{\text{tot}}(E) + \mu_{\text{tot}}(E_f) g} \quad . \tag{3}$$

The spectra are angle dependent via the geometry factor $g := \sin(\alpha)/\sin(\beta)$. Thus, if measurements are carried out at different geometries g_1 and g_2, different spectra $I_1^X(E)$ and $I_2^X(E)$ will be observed. Using the normalized experimental spectra $I_i(E) := I_i^X(E)/I_{0i}(E)$ and $c_i^{-1} := \eta \frac{A_i}{r_i^2} \omega_X$ the two spectra can be described as

$$I_1 = c_1^{-1} \frac{\mu_X(E)}{\mu_{\text{tot}}(E) + \mu_{\text{tot}}(E_f) g_1} \tag{4}$$

and

$$I_2 = c_2^{-1} \frac{\mu_X(E)}{\mu_{\rm tot}(E) + \mu_{\rm tot}(E_f) g_2} \quad . \tag{5}$$

These equations can be solved for the absorption coefficients:

$$\mu_{\rm tot}(E) = \mu_{\rm tot}(E_f) \frac{g_2 c_2 I_2(E) - g_1 c_1 I_1(E)}{c_1 I_1(E) - c_2 I_2(E)} \tag{6}$$

and

$$\mu_X(E) = \mu_{\rm tot}(E_f)(g_2 - g_1) \frac{c_1 I_1(E)\, c_2 I_2(E)}{c_1 I_1(E) - c_2 I_2(E)} \quad . \tag{7}$$

By determining the quantities $I_i(E)$, g_i, and c_i the the absorption coefficients can be evaluated relative to $\mu_{\rm tot}(E_f)$. $I_i(E)$ and g_i are directly measurable, and below we will discuss how the uncertainty in c_i can be taken into account.

Note that in Eq. (7), the geometry factors g_i are only scaling the spectrum and do not affect its shape. This means that one does not have to accurately determine the geometries. Any two spectra recorded at different angles will produce the same μ_X *shape* as evaluated by Eq. (7). However, as the information depth changes as a function of the angle, for inhomogenous samples two geometries corresponding to the same information depth should be chosen. This is discussed in more detail in Sec. IV. It must also be noted that it is helpful to choose geometries resulting in two significantly different experimental spectra to minimize errors due to the denominator of Eq. (7). A second advantage of Eq. (7) is that it is valid not only on the high-energy side of an absorption edge, but also below the edge. If the photon energy is lowered below the threshold value, all measured intensities drop to zero. While Eq. (6) is no longer defined in this limit, Eq. (7) still holds, as the numerator approaches zero quadratically in contrast to the denominator.

In the case where $c_1 = c = c_2$, Eq. (7) can be written as

$$\mu_X(E) = \mu_{\rm tot}(E_f)(g_2 - g_1) c \frac{I_1(E)\, I_2(E)}{I_1(E) - I_2(E)} \quad ; \tag{8}$$

i.e., the shape is neither affected by the geometry factors g_i nor by the proportionality factor c.

However, it can be experimentally difficult to fulfill the condition $c_1 = c_2$. If that is not possible, c_1 and c_2 have to be determined in order to use the expressions (6) and (7).

This problem can be solved by using assumptions about $\mu_{\rm other}$. If the level of interest X is separated far enough in energy from adjacent core levels, it is a good approximation to use $\mu_{\rm other} = {\rm const}$ on the narrow energy range of interest in XANES. If one can further assume that all the emission falls below the absorption edge, this constant equals $\mu_{\rm tot}(E_f)$:

$$\mu_{\rm tot}(E) = \mu_X(E) + \mu_{\rm tot}(E_f) \quad . \tag{9}$$

Using Eqs. (6) and (7), Eq. (9) can be rewritten as

$$c_1 = \frac{I_2(E)(1 + g_2) - \frac{c_1}{c_2} I_1(E)(1 + g_1)}{I_1(E) I_2(E)(g_2 - g_1)} \quad . \tag{10}$$

As c_1 and c_2 must be independent of energy, this equation can be used to determine these factors. The ratio c_1/c_2 has to be varied as a parameter until c_1 is constant as a function of energy.

Using this method, it is easy to evaluate $c_{1,2}$ with sufficient accuracy so that the formulas (6) and (7) can be used to determine the absorption coefficients. It must be noted that this procedure depends on the determination of the correct values for g_i.

III. EXPERIMENTAL DETAILS

Soft-x-ray near-edge absorption spectra were recorded for the Co L_3 edges of various samples using the 1221 lines/mm grating of the SX700-2 monochromator at the BESSY synchrotron facility, Berlin. Using a 45-μm exit slit, the energy resolution is about 1.2 eV at 780 eV photon energy. The photon flux was determined by a high-transmission gold mesh. Fluorescence radiation was detected 90° from the incident-beam direction by a Ge solid-state detector coupled to a multichannel analyzer resulting in an energy resolution of 100 eV at a photon energy of 780 eV. Thus we were able to select the Co $L_{2,3}$ radiation in a partial-yield mode. Additionally to this partial fluorescence yield, the total electron yield was recorded by a channeltron, 45° from the beam direction. As the detector was always 90° from the beam direction in our setup, the geometry factor is given by $g := \frac{\sin\alpha}{\sin\beta} = \tan\alpha$.

We demonstrate that the method described in Sec. II gives the same results as EY for polished and sputtered Co metal and a $CoSi_2$ single crystal and apply the method to an ion-beam-synthesized $CoSi_2$ layer[6] of 50 nm thickness buried below the surface of a Si wafer.

IV. RESULTS AND DISCUSSION

To illustrate the effects associated with self-absorption in the fluorescence-yield detection of XANES for concentrated samples, Fig. 2 shows a simulation of the basic equation (3) for Co, in the experimental geometry described above, using EY data as input for μ_X. Here $\mu_{\rm tot}(E_f)$ was estimated to be 14% of the total rise of the total absorption coefficient over the $L_{2,3}$ edges[7,8] and the validity of Eq. (9) was assumed. As the total intensity decreases with increasing glancing angle, the calculated FY spectra and the EY input data have been scaled to the L_3 edge jump in Fig. 2. Besides the fact that the overall signal gets more intense in grazing incidence, the main effect of the self-absorption is to enhance low-signal regions of the spectrum under the grazing-incidence conditions. As high-signal regions of the spectrum are less enhanced, the spectral features are more and more "washed out" if a setup with more grazing incidence is chosen. Thus the spectrum appears to be saturated. The absorption edge is broadened due to this enhancement of low-signal regions and appears to be shifted to lower energies for

lower g values. Consequently it is of utmost importance to correct for these effects when electron binding energies are to be determined.

For $g \rightarrow \infty$, which corresponds to a normal-incidence grazing-takeoff geometry, the FY signal approaches the real absorption spectrum, a fact which has been used to record FY spectra.[4] This is always true, if $(\mu_{\mathrm{tot}}(E_f)\, g)$ dominates the denominator of Eq. (1). If on the other hand $\mu_{\mathrm{tot}}(E) \gg (\mu_{\mathrm{tot}}(E_f)\, g)$, the saturation effect can still be small if $\mu_{\mathrm{tot}}(E) \gg \mu_X(E)$. This condition defines the dilute sample limit, where μ_{other} is high due to the presence of other atomic species. The smaller μ_{other} gets, the stronger is the saturation effect in the FY spectra, leading to a completely saturated signal in the extreme case where $\mu_{\mathrm{tot}}(E) = \mu_X(E)$. Thus a geometry characterized by a sufficiently high g has to be chosen to monitor the absorption if the data is not corrected for these effects. Then, however, count rates are lower due to the strong self-absorption.

In Fig. 3 experimental data for the Co L_3 absorption edge of a polished and sputtered Co sample are shown, demonstrating the effect of self-absorption in the FY spectra. Two FY spectra recorded at different geometries are compared to the EY signal. Because of the small escape depth even for inelastically scattered electrons, the EY signal can be assumed to be proportional to the absorption coefficient of Co. The prominent peak visible can be related to the density of unoccupied electronic states of d symmetry at the Co atom.

The calculated self-absorption effects as presented in Fig. 2 are clearly visible in the experimental spectra. The grazing-incidence (glancing angle $\alpha = 27.0°$, $g = 0.51$) FY spectrum differs clearly from the EY spectrum. The pre-edge signal is enhanced, resulting in a broadening of the peak and an apparent shift of the edge. In contrast to the real absorption coefficient, the intensity does not drop significantly on the high-energy side of the absorption edge. In the normal-incidence (glancing angle $\alpha = 85.0°$, $g = 11.4$) FY spectrum the saturation effects are smaller, but the signal is still not proportional to the absorption coefficient as measured by total EY, demonstrating the need to correct for the angle dependence of the FY spectra.

The two FY spectra as shown in Fig. 3 have been used to calculate the total absorption coefficient $\mu_{\mathrm{tot}}(E)$ and the absorption coefficient $\mu_{L_3}(E)$ assocciated with the production of the Co $2p_{\frac{3}{2}}$ core hole using Eqs. (6), (7), and (10). The results are shown in Fig. 4. The absorption coefficients are plotted in units of the total absorption coefficient below the L_3 threshold $\mu_{\mathrm{tot}}(E_f)$. As expected, the two spectra differ only by an additive constant. As this behavior was assumed by using Eqs. (9) and (10) to determine the constants c_i, this demonstrates the self-consistency of the procedure.

Note that $\mu_{\mathrm{tot}}(E)$ calculated according to Eq. (6) is more influenced by the uncertainties of the two input data sets than $\mu_{L_3}(E)$. As pointed out in Sec. II, Eq. (6) used to calculate $\mu_{\mathrm{tot}}(E)$ is not well defined below the absorption threshold; consequently the plotted $\mu_{\mathrm{tot}}(E)$ curve is not correct in this energy range. This results in a large variation and an incorrect offset of the $\mu_{\mathrm{tot}}(E)$ curve relative to $\mu_{L_3}(E)$ in the pre-edge region. Nevertheless, if the post-edge offset of the two absorption coefficients is used, the pre-edge value of the total absorption coefficient can be determined approximately as $\mu_{\mathrm{tot}}(E = 771\ \mathrm{eV}) \simeq \mu_{\mathrm{tot}}(E_f)$, again demonstrating the self-consistency of the

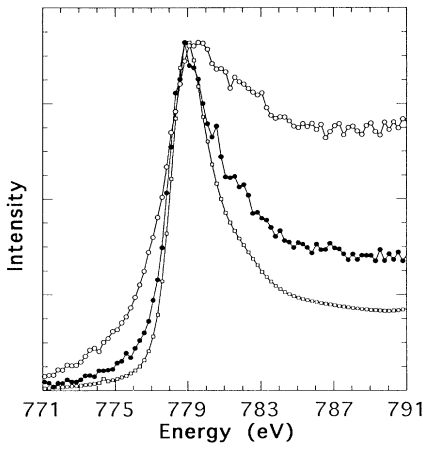

FIG. 3. Co L_3 XANES as detected by EY (squares) and FY (circles) as a function of photon energy. Intensities have been normalized to the L_3 peak. FY spectra have been recorded for two different experimental geometries: glancing angle of incidence 27.0° (open circles) and 85.0° (solid circles). Strong saturation effects are present in the 27.0° spectrum: Low-signal regions appear to be enhanced. The saturation effects are reduced in the 85.0° geometry but are still distorting the shape of the spectrum, as indicated by comparison with the EY data.

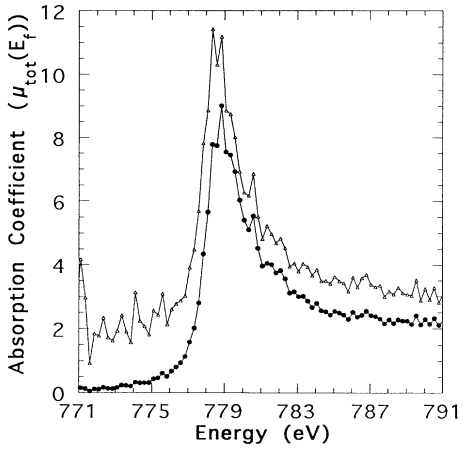

FIG. 4. Total absorption coefficient μ_{tot} (open triangles) and the absorption coefficient associated with the creation of a Co $2p_{\frac{3}{2}}$ core hole μ_{L_3} (solid circles) as a function of photon energy. One unit on the y axis corresponds to the total absorption coefficient at the fluorescence photon energy E_f. The spectra have been calculated from the FY data in Fig. 3 using Eqs. (6), (7), and (10).

analysis. It can be estimated that $\mu_{\rm tot}(E)$ increases by a factor of 4.5 ± 1.5 when the energy is varied over the Co L_3 *and* L_2 edges, which is slightly lower than other values reported.[7,8,10]

The *absolute* values of the absorption coefficients calculated in this way depend on a correct determination of the experimental geometry. In our measurements the angle of incidence was determined to an accuracy of 1°. The uncertainty in the takeoff angle due to the acceptance of the detector was 10° for the closest detector position. We estimate the resulting error for the determination of absolute values of the absorption coefficient to be about 50%.

However, in most experiments relating the XANES to the electronic structure the correct *shape* of the absorption coefficient is of primary importance. Thus the derived $\mu_{L_3}(E)$ absorption coefficients will be used in further discussions, because (a) this is the physical property of interest with respect to the electronic structure determination in XANES, (b) $\mu_{L_3}(E)$ as determined by Eq. (7) is well defined over the whole energy range, and (c) it is not as sensitive on the statistical scattering of the input data as $\mu_{\rm tot}(E)$.

In Fig. 5 the FY derived $\mu_{L_3}(E)$ for Co is compared to the EY signal. Compared to the uncorrected normal-incidence FY spectrum presented in Fig. 2 the improvement is obvious: $\mu_{L_3}(E)$ as derived from the angular dependence of the FY as outlined above fits very well to the EY spectrum. Assuming a constant branching ratio between the fluorescent and the nonfluorescent relaxation channels across the energy range of interest, the agreement between FY and EY supports the validity of the analysis method. Both the L_3-edge position as well as the overall shape are reproduced, when the error due to the statistics and the determination of the geometry factors are taken into account. The uncertainty due to the angle measurement is indicated by the error bars. Their top and bottom points represent the derived absorption coefficients, if the angle of incidence is ±1° off the value used for the dotted spectrum. Even for a detector position close to the sample, the error due to the detector acceptance angle is slightly smaller. It could be reduced by placing a slit in front of the detector in future experiments.

Note that this angular dependence is not given by Eq. (7) itself. It enters indirectly via the use of Eq. (9) to determine the proportionally factors $c_i := (r_i^2)/(A_i \eta \omega_{L_3})$ in the two FY spectra as described in the theory section. This method is illustrated in Fig. 6 showing the value c_1, the constant of proportionality for the grazing-incidence FY spectrum, after the parameter c_1/c_2 has been varied to find the best value characterized by the condition $c_1(E) = \text{const}$. This condition is clearly fulfilled in the energy range above 779 eV, i.e., above the absorption coefficient peak energy, allowing us to determine c_1 and c_2 with sufficient accuracy. The possible error due to this method is estimated to be smaller than the consequences of an erroneous angle determination as depicted in Fig. 5. The scattering of c_1 on the low-energy side of the L_3-absorption threshold ($E < 776$ eV) indicates the fact that Eq. (9) is not well defined in this energy range as mentioned above. It is impossibe to find a parameter c_1/c_2 in such a way that c_1 is constant between 776 eV and 779 eV. We do not have an unambiguous explanation for this observation.

In Fig. 7 we present data on a system where the deep-

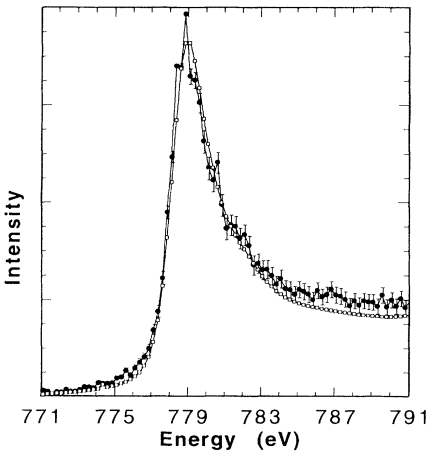

FIG. 5. Co L_3 XANES spectrum derived from the FY measurement (solid circles) as presented in Fig. 4 compared to the EY spectrum (open squares). The FY derived spectrum is in good agreement with the EY spectrum, when the uncertainty due to the statistics and the determination of the experimental geometry are taken into account. The error bars illustrate the influence of an erroneous determination of the experimental geometry on the shape of the derived XANES spectrum. They represent the absorption coefficients derived, if the angle of incidence is ±1° different from the value used for the calculation of the dotted spectrum.

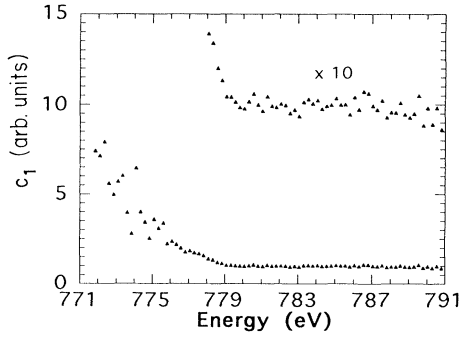

FIG. 6. In this picture we illustrate the method relying on Eq. (10) to determine the constants of proportionality c_i as described in Sec. II. These constants are inversely proportional to the fluorescence yield, the detection efficiency, and the solid angle covered by the fluorescence detector. They have to be determined in order to calculate the absorption coefficient from the two FY spectra recorded at different angles. For the Co system, the c_1 value corresponding to the grazing-incidence spectrum is shown as a function of photon energy, after the parameter c_1/c_2 has been varied according to Eq. (10) to fulfill the condition $c_1(E) = \text{const}$. See text for a more detailed discussion.

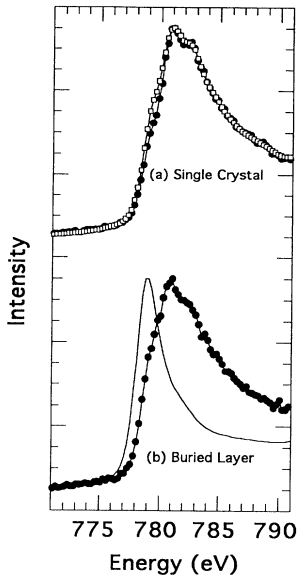

FIG. 7. In this figure we compare Co L_3 XANES spectra derived by EY (open squares) and by the angular dependence of the FY (solid circles) for a $CoSi_2$ single crystal (a) and a $CoSi_2$ layer of 500 Å thickness buried in a silicon wafer produced by means of ion-beam synthesis (IBS) (Ref. 6). For comparison, EY data for Co is included in (b) (solid line). The clear $CoSi_2$ XANES fingerprint observed for the buried layer by FY detection indicates that indeed $CoSi_2$ is produced in the IBS process and that it is possible to investigate such buried layers *in situ* by the deep-probing FY technique.

probing FY technique has to be used in order to obtain XANES spectra. In Fig. 7(a) we compare the EY signal of a $CoSi_2$ single crystal to $\mu_{L_3}(E)$. Excellent agreement between the two different methods can be seen: Both show a double-peak structure at about 781 eV and 783 eV, respectively, as well as a low-energy shoulder at about 779 eV. In this case, the angular dependence of the FY measurements has been used to check whether our normal-incidence spectrum, recorded at 89.0° glancing angle, is distorted due to saturation effects. We can show that the corrections are negligible in this geometry.

For this $CoSi_2$ single crystal the same XANES spectrum can be obtained using the EY technique. This does not work for the second sample, a $CoSi_2$ layer of 500 Å thickness buried below the surface of a silicon wafer by means of ion-beam synthesis[6] [Fig. 7(b)]. Here the deep-probing FY method shows a clear $CoSi_2$ single-crystal fingerprint, including the low-energy shoulder and the double-peak structure. Again, using the angle dependence of the FY spectra we could prove that the corrections to the normal-incidence spectrum recorded at 89.4° glancing angle are negligible. The interpretation of the spectra in terms of the electronic structure will be presented in a separate publication.[9]

We will now investigate the information depth of the technique. The probability to detect a fluorescence photon generated in the depth x perpendicular to the surface is described by

$$P(x) \propto \exp\left[-\left(\frac{\mu_{\rm tot}(E)}{\sin\alpha}+\frac{\mu_{\rm tot}(E_f)}{\sin\beta}\right)x\right] \quad . \tag{11}$$

The information depth λ_f of the FY detection can be defined as the expectation value of x with respect to this probability distribution:[5]

$$\lambda_f := \frac{\int_0^\infty xP(x)dx}{\int_0^\infty P(x)dx} \tag{12}$$

$$= \frac{\sin\alpha}{\mu_{\rm tot}(E)+\mu_{\rm tot}(E_f)g} \quad . \tag{13}$$

Figure 8 shows the information depth for pure Co as a function of the glancing angle α (see Fig. 1, $\alpha+\beta=90°$) for two different energies. The information depth is limited by the absorption of the generated fluorescence photons for glancing angles close to 90° and by the absorption of the incident photons for small glancing angles. Consequently, the information depth has a maximum at intermediate angles. The asymmetry is caused by the fact that $\mu_{\rm tot}(E_f)$ is smaller than $\mu_{\rm tot}(E)$, if the energy E is above the absorption edge.

As $\mu_{\rm tot}(E)$ shows a strong variation in the XANES region (inset in Fig. 8), the information depth is energy dependent. Curve (a) shows the information depth for an energy 13 eV above the absorption edge while (b) shows the information depth at the energy corresponding to the strongest absorption.

For the first case, the information depth maximum of about 700 Å is obtained for a glancing angle of about 60°.

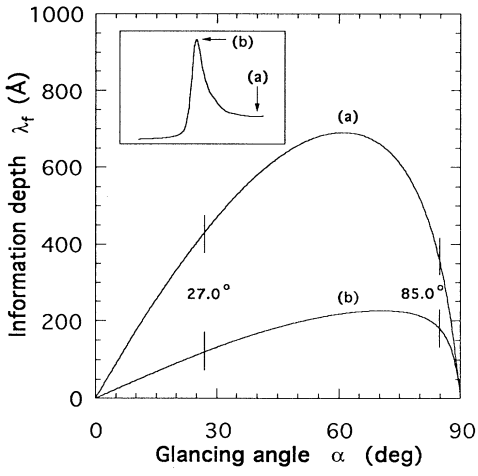

FIG. 8. This figure shows the information depth λ_f as a function of the angle of incidence for Co in our experimental setup ($\alpha+\beta=90°$). The information depth varies with photon energy due to the variation of the absorption coefficient over the Co L_3 edge shown in the inset. Thus the information depth has been calculated for the maximum absorption (b) and for an absorption value above the L_3 edge (a). The angles of incidence chosen for the two FY spectra to derive the Co XANES are indicated (see Fig. 3).

In the second case, the information depth is considerably reduced to a maximum value of 225 Å, peaking at 70°. Thus one has to be aware that the information depth changes as a function of $\mu_{\text{tot}}(E)$ while scanning a XANES spectrum of a concentrated sample in the FY detection mode.

In order to derive the absorption coefficient as outlined in Sec. II, two measurements at different angles have to be made. Because of shape of the information depth as a function of the glancing angle, it is always possible to choose two geometries which correspond to the same information depth. The angles used for the measurements on Co presented in Sec. IV are indicated in Fig. 8. They correspond to a maximum information depth of about 400 Å [(a)] and a minimum information depth of about 175 Å [(b)]. Thus we are bulk sensitive in our measurements.

For the buried $CoSi_2$ layer, the information depth calculated in this way starts at the beginning of the buried layer. As no Si-absorption edges are present in the energy range investigated, this can be regarded as constant over the spectral energy range. Additionally, there is no contribution to the fluorescence signal originating from this Si cap layer.

Thus, the influence of the silicon coverlayer can be described as simlply reducing the incident photon flux and the detection efficiency for the fluorescence photons. Consequently, the spectral shape remains unaffected by the coverlayer; only the intensity is reduced. This reduction can be calculated if the thickness of the coverlayer is known. However, this intensity scaling is automatically accounted for if the proportionallity factors c_i are determined using Eq. (10) as described in Sec. II.

V. CONCLUSIONS

We presented a method to determine the absorption coefficient in the XANES energy range for concentrated samples by monitoring the fluorescence yield. The method uses the fact that it is possible to describe the angular dependence of the absorption processes occuring in this photon-in–photon-out type of spectroscopy analytically.

Making measurements at two different experimental geometries, it is possible to calculate the absorption coefficient. Thus we are able to correct for the saturation effects often present in FY-derived spectra of concentrated samples. The technique was demonstrated for a pure Co sample.

The information depth of the method was investigated and found to be large enough to measure real bulk properties of the sample. By FY detection, it is possible to study buried layers which are unaccessible by conventional electron spectroscopies. This has been demonstrated for a $CoSi_2$ layer buried below the surface of a silicon wafer.

ACKNOWLEDGMENTS

We would like to thank R. Jebasinski and S. Mantl for providing the buried silicide samples and U. Döbler for providing the $CoSi_2$ single crystal. We are grateful to K. Holldack for his help with the fluorescence chamber and to G. Remmers and M. Domke for helping out at the SX-700-II at BESSY, Berlin.

[1] A. Krol, C.S. Lin, Z.H. Ming, C.J. Sher, Y.H. Kao, C.T. Chen, F. Sette, Y. Ma, G.C. Smith, Y.Z. Zhu, and D.T. Shaw, Phys. Rev. B **42**, 2635 (1990).

[2] J. Jaklevic, J.A. Kirby, M.P. Klein, A.S. Robertson, G.S. Brown, and P. Eisenberger, Solid State Commun. **23**, 679 (1977).

[3] E. Zschech, L. Tröger, D. Arvanitis, H. Michaelis, U. Grimm, and K. Baberschke, Solid State Commun. **82**, 1 (1992).

[4] D.M. Pease, D.L. Brewe, Z. Tan, and J.I. Budnick, Phys. Lett. A **138**, 230 (1989).

[5] L. Tröger, D. Arvanitis, K. Baberschke, H. Michaelis, U. Grimm, and E. Zschech, Phys. Rev. B **46**, 3283 (1992).

[6] R. Jebasinski, S. Mantl, L. Vescan, and Ch. Dieker, Appl. Surf. Sci. **53**, 264 (1991).

[7] J.J. Yeh and I. Lindau, At. Data Nucl. Data Tables **32**, 47 (1985).

[8] B.L. Henke, P. Lee, T.J. Tanaka, R.L. Shimabukuro, and B.K. Fujikawa, At. Data Nucl. Data Tables **27**, 1 (1982).

[9] S. Eisebitt, T. Böske, J.-E. Rubensson, R. Jebasinski, S. Mantl, J. Kojnok, P. Skytt, J. Guo, N. Wassdahl, J. Nordgren, K. Holldack, and W. Eberhardt (unpublished).

[10] W.J. Veigele, in *Handbook of Spectroscopy*, edited by J.W. Robinson (CRC, Cleveland, 1974), Vol. 1.